Black-Hole Remnants from Black-Hole–Neutron-Star Mergers

Francesco Zappa,[1] Sebastiano Bernuzzi,[1] Francesco Pannarale,[2,3] Michela Mapelli,[4,5,6,7] and Nicola Giacobbo[4,5,6]

[1]*Theoretisch-Physikalisches Institut, Friedrich-Schiller-Universität Jena, 07743 Jena, Germany*
[2]*Dipartimento di Fisica, Università di Roma "Sapienza", Piazzale A. Moro 5, I-00185 Roma, Italy*
[3]*INFN Sezione di Roma, Piazzale A. Moro 5, I-00185 Roma, Italy*
[4]*Physics and Astronomy Department Galileo Galilei, University of Padova, Vicolo dell'Osservatorio 3, I-35122 Padova, Italy*
[5]*INAF-Osservatorio Astronomico di Padova, Vicolo dell'Osservatorio 5, I-35122 Padova, Italy*
[6]*INFN-Padova, Via Marzolo 8, I-35131 Padova, Italy*
[7]*Institut für Astro- und Teilchenphysik, Universität Innsbruck, Technikerstrasse 25/8, A-6020 Innsbruck, Austria*

Observations of gravitational waves and their electromagnetic counterparts may soon uncover the existence of coalescing compact binary systems formed by a stellar-mass black hole and a neutron star. These mergers result in a remnant black hole, possibly surrounded by an accretion disk. The mass and spin of the remnant black hole depend on the properties of the coalescing binary. We construct a map from the binary components to the remnant black hole using a sample of numerical-relativity simulations of different mass ratios q, (anti)aligned dimensionless spins of the black hole a_{BH}, and several neutron star equations of state. Given the binary total mass, the mass and spin of the remnant black hole can therefore be determined from the three parameters (q, a_{BH}, Λ), where Λ is the tidal deformability of the neutron star. Our models also incorporate the binary black hole and test-mass limit cases and we discuss a simple extension for generic black-hole spins. We combine the remnant characterization with recent population synthesis simulations for various metallicities of the progenitor stars that generated the binary system. We predict that black-hole–neutron-star mergers produce a population of remnant black holes with masses distributed around 7 $M_\odot$ and 9 $M_\odot$. For isotropic spin distributions, nonmassive accretion disks are favored: no bright electromagnetic counterparts are expected in such mergers.

Introduction.—Mergers of a stellar-mass black hole (BH) and a neutron star (NS), hereafter BHNS, are expected sources of gravitational waves (GWs) detectable by ground-based laser interferometers and possibly accompanied by electromagnetic counterparts [1–7]. No GW observations of BHNS binaries have been made to date. The 90% confidence upper limit on their merger rate is 610 Gpc^{-3} yr^{-1} [8]. To prepare these observations, quantitative general-relativistic theoretical models of the GW and merger outcome are required. Throughout this work we use geometric units $c = G = 1$ unless otherwise stated.

Numerical-relativity (NR) simulations of BHNSs are the only means to study BHNS mergers [2–4,9–18]. Simulations indicated that the NS tidal disruption is a characteristic feature of the dynamics of quasicircular BHNS mergers. On the contrary, quasicircular binary NS mergers with mass ratio up to ~2 do not present significant tidal disruption; see, e.g., Refs. [19,20]. Tidal disruption happens if the NS reaches a characteristic distance r_{TD} from the BH before the innermost stable circular orbit (ISCO), the radius of which we denote by r_{ISCO}. r_{TD} is expected to scale in the same way as the radius at the onset of mass shedding r_{MS}, which is determined by the condition that the BH tidal force overcomes the NS self-gravity at the stellar surface

R_{NS}. Defining the binary mass ratio $q = M_{BH}/M_{NS}$, this condition implies $r_{TD} \lesssim r_{MS} \propto q^{1/3} R_{NS}$, with a weak dependency on the BH spin [21]. In the test-mass limit of a particle orbiting a Kerr BH of mass M_{BH}, $r_{ISCO} = M_{BH} f(a_{BH})$, where $f(a_{BH}) \in [1, 9]$ is a monotonically decreasing function of the BH dimensionless spin parameter a_{BH} [22] (The dimensionless parameter range is $a_{BH} \in [-1, 1]$ accounting for antialigned and aligned spins). Because $R_{NS}/M_{BH} = (qC)^{-1}$, where $C = M_{NS}/R_{NS}$ is the NS compactness, the ratio that regulates the onset of tidal disruption is $\xi = r_{TD}/r_{ISCO} \propto C^{-1} q^{-2/3} f(a_{BH})^{-1}$. Thus, tidal disruption depends on three physical parameters: the binary mass ratio, the BH spin, and the NS compactness. The above conclusion is expected to hold also for finite mass ratios, in which case the tidal disruption is determined by the binary's tidal and spin-orbit interactions.

Simulations have shown that tidal disruption occurs for BHNSs with $q \lesssim 3$ if the BH is nonspinning, or its spin is antialigned with the orbital angular momentum. Generally speaking, large, aligned BH spins $a_{BH} \gtrsim +0.5$ favor tidal disruption because spin-orbit interactions push the ISCO radius to smaller values. As an example, $r_{ISCO} = 1M_{BH}$ for a Kerr BH with $a_{BH} = +1$, as opposed to $r_{ISCO} = 6M_{BH}$ for a nonspinning BH. Disruption is also favored by low

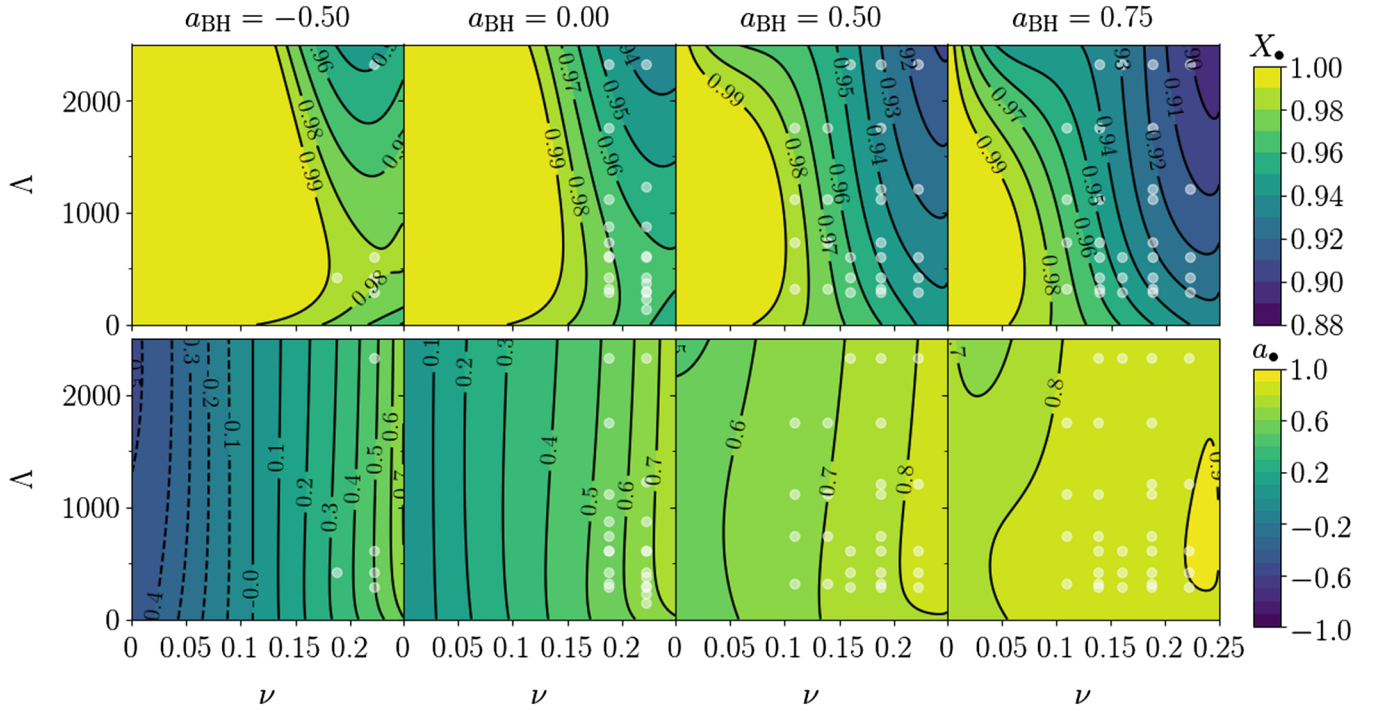FIG. 1.   Contour plots of the remnant BH mass divided by the binary mass $X_\bullet = M_\bullet/M$ (top) and of the dimensionless spin parameter $a_\bullet$ (bottom) as a function of the symmetric mass ratio ν and of the NS tidal polarizability parameter Λ, at fixed values of the initial BH spin parameter $a_{\rm BH}$. The values of $a_{\rm BH}$ correspond to those of the NR simulations. No assumptions on the EOS are made for the NS, which is characterized solely by Λ. White markers indicate the NR data used to construct the model.

values of the NS compactness, which are related to stiff equations of state (EOSs), that also imply large NS tidal deformabilities [23,24]. Note that, for a fixed NS mass, large deformabilities imply large NS radii and small binary mass ratios correspond to small BH masses.

Tidal disruption leads to the formation of an accretion disk in the merger remnant. Simulations predict remnant disks with baryon (rest) masses as large as $\gtrsim 0.1\,M_\odot$ [25,26], thus creating the conditions to ignite a short gamma-ray burst (SGRB) [27–29]. Kyutoku *et al.* [2] tentatively classify the phenomenology of BHNS mergers into three classes, based on the ratio ξ. For type-I and type-III mergers, tidal disruption occurs far from or close to the ISCO; for type-II mergers, it does not occur and the NS plunges onto the BH, because the tidal disruption radius is located well within the ISCO. The three classes differ by their GW spectra and the disk masses. Type-II mergers are typically characterized by $q \gtrsim 3$, $a_{\rm BH} \lesssim 0$ and have a GW spectrum very similar to binary black holes (BBHs); see, e.g., Refs. [30–34].

An analytical formula for the BH remnant mass and dimensionless spin can be found using mass and angular momentum conservation arguments [35,36] (see also Ref. [37]). That approach builds on estimates of the radiated energy and the binary orbital angular momentum based on the expressions for test particles on Kerr background at ISCO, and on the disk mass fits of Ref. [25]. Results are accurate to a few percent, which is comparable

to the energy radiated in GWs. The largest uncertainty comes from the disk mass estimates in simulations; see, e.g., Refs. [26,38].

In this work we model the remnant of BHNSs using NR data. Using a state-of-the-art synthetic population, we predict that the most likely BHNS mergers are of type II, leading to a population of light remnant BHs.

Remnant mass and spin.—Given the gravitational binary mass $M = M_{\rm BH} + M_{\rm NS}$, we map the remnant mass and spin parameters of BHNS mergers as follows:

$$F: (\nu, a_{\rm BH}, \Lambda) \to (X_\bullet, a_\bullet), \qquad (1)$$

where $X_\bullet = M_\bullet/M$ and $a_\bullet = S_\bullet/M_\bullet^2$, $M_\bullet$ and $S_\bullet$ being the mass and spin of the remnant BH, respectively. Above, $\nu = q/(1+q)^2 \in [0, 1/4]$ is the symmetric mass ratio ($q = M_{\rm BH}/M_{\rm NS} \geq 1$), spanning from the test-mass ($\nu = 0$) to the equal-mass ($\nu = 1/4$) limit. $a_{\rm BH}$ is the dimensionless spin of the initial BH, that is aligned with the binary orbital angular momentum. The quantity Λ is the dimensionless NS quadrupolar tidal polarizability parameter [23], $\Lambda = 2k_2/(3C^5)$, where k_2 is the gravitoelectric quadrupolar Love number, a monotonically decreasing function of the compactness C [24]. Λ describes tidal interactions at the leading order in post-Newtonian dynamics. Typically, $\Lambda \sim 100$–2500 for NSs in BHNS systems, depending on the NS mass and equation of state.

We use data of NR simulations of quasicircular BHNS mergers described in Refs. [2,9,11] and collected in the Supplemental Material (SM) [39]. These simulations adopt different neutron star matter EOSs and (anti)aligned BH spin values.

The NS spin, on the contrary, is neglected and currently not accounted for in our models; however, this is expected to be a good approximation of realistic systems [44,45].

The data cover the following parameter intervals: $\Lambda \in [100, 2500]$, $\nu \in [0.109, 0.222]$ (in terms of q, this interval translates into $q \in [2, 7]$), and $a_{\mathrm{BH}} \in [-0.5, 0.75]$. The mapping F is summarized in Fig. 1; technical details on its construction are provided in the SM [39].

The remnant BH mass scaled to M is given by

$$X_{\bullet} = 1 - \frac{E_{\mathrm{GW}}}{M} - \frac{M_{\mathrm{disk}}}{M} - \frac{M_{\mathrm{ejecta}}}{M}, \qquad (2)$$

where E_{GW} is the total energy radiated in GWs during the coalescence and M_{disk} and $M_{\mathrm{ejecta}} \lesssim 0.08\,M_{\odot} < M_{\mathrm{disk}}$ are the disk and mass-ejecta contribution to the gravitational energy which cannot be directly measured in the simulations [11]. Note that the measurements of $X_{\bullet}$ and $a_{\bullet}$ are performed from the apparent horizon in the simulations. In BBH mergers finite mass-ratio effects are repulsive, implying that the GW emission is more efficient for larger ν. The same effect is present in the BHNS dynamics: Figure 1 shows that the smallest values of $X_{\bullet}$ are obtained for larger values, $\nu \to 1/4$. The precise behavior of $X_{\bullet}$, however, depends on the competition between the energy emitted in GWs and the effect of tidal disruption, as per Eq. (2). For nonspinning BHNS binaries (second column in Fig. 1), one observes that the value of $X_{\bullet}$ slightly increases with respect to the BBH case as $\Lambda > 0^+$ and for a given ν. Tidal disruption does not occur for small values of Λ (e.g., $\Lambda \lesssim 500$ for $\nu = 0.22$ and $a_{\mathrm{BH}} = 0$), so this effect is solely due to the fact that tidal interactions are attractive and reduce the emission of GWs with respect to the $\Lambda = 0$ case (i.e., E_{GW} decreases so $X_{\bullet}$ grows, with $M_{\mathrm{disk}} \simeq 0$). As Λ becomes sufficiently large (and $\nu \to 1/4$), tidal disruption occurs and only part of the remnant mass contributes to the final BH mass. Consequently, as Λ increases beyond a certain critical value, $X_{\bullet}$ starts to decrease because part of the NS mass is not swallowed by the BH but becomes part of the disk. Note that the peak mass is more pronounced for $\nu \to 1/4$ and disappears for sufficiently small ν (type-II mergers).

Focusing on spin effects, at a given ν, the remnant mass decreases for increasing $a_{\mathrm{BH}} > 0$ because the ratio ξ increases. This is a consequence of the repulsive character of the spin-orbit interaction for aligned (positive) spins. Notably, the peak for small Λ is no longer present for sufficiently large values of a_{BH}. For $a_{\mathrm{BH}} < 0$, the spin-orbit interactions are attractive; i.e., they have the same sign as tidal interactions. As a consequence, for smaller a_{BH}'s, $X_{\bullet}$ increases and the peak at small Λ is more pronounced.
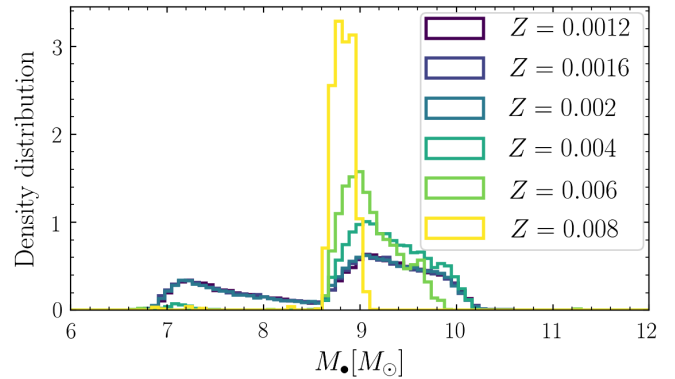

FIG. 2. The remnant BH mass distribution inferred from the remnant to a different value of the metallicity Z of the progenitor stars. In this plot we employ the SLy EOS and the fiducial isotropic spin distribution peaked around $\langle a_{\mathrm{BH}} \rangle = 0.2$.

For nonspinning BBHs, the remnant BH spin $S_{\bullet}$ is expected to decrease for increasing ν, due to the same finite mass-ratio effect described above. Because of the $M_{\bullet}^2$ normalization, however, $a_{\bullet}$ shows the opposite behavior. In the BHNS case, the remnant BH has a larger dimensionless mass-rescaled spin with respect to the BBH case and it increases with Λ, for small $\Lambda > 0$. This happens because the NS compactness is smaller and less angular momentum is dissipated via GWs. Above a peak value, however, tidal disruption occurs and the angular momentum redistributes into the disk that forms around the remnant BH.

For $|a_{\mathrm{BH}}| \lesssim 0.5$ and a given value of ν, the final $a_{\bullet}$ is roughly linear in a_{BH} [see Eq. (4) in SM [39] and Ref. [2]]. For $a_{\mathrm{BH}} \gtrsim +0.75$, one recovers $a_{\bullet} \sim a_{\mathrm{BBH}}$, as expected.

Although our models are developed from nonprecessing BHNS data, they can be extended to the case of generic BH spins [36,46,47]. The simplest extension—which we adopt—is to map the initial spin,

$$a_{\mathrm{BH}} \to a_{\mathrm{BH}} \cos\beta = a_{\mathrm{BH}}^z, \qquad (3)$$

where β is the angle between the initial BH spin and the orbital angular momentum $\mathbf{L}$. In this case the model will yield $a_{\bullet}^z$ instead of $a_{\bullet}$. This prescription also assumes that the direction of the total angular momentum $\mathbf{J} = \mathbf{L} + \mathbf{S}$ is approximately preserved and so the direction θ of the final spin is given by the projection $\cos\theta = \hat{\mathbf{J}} \cdot \hat{\mathbf{L}}$. Predictions in the precessing case agree with the simulations of Ref. [13] (see SM [39]).

Binary and remnant population.—We now apply the formalism described in the previous section to a BHNS population merging at redshift $z \leq 1$ and constructed by convolving the binary population synthesis from the MOBSE code [48–50] with the Illustris cosmological simulation [51–53] (see Refs. [54–56] and the SM [39] for details). In particular, we adopt run CC15α5 of Ref. [56], where the common-envelope parameter is $\alpha = 5$ and natal kicks are drawn from a Maxwellian distribution with a single
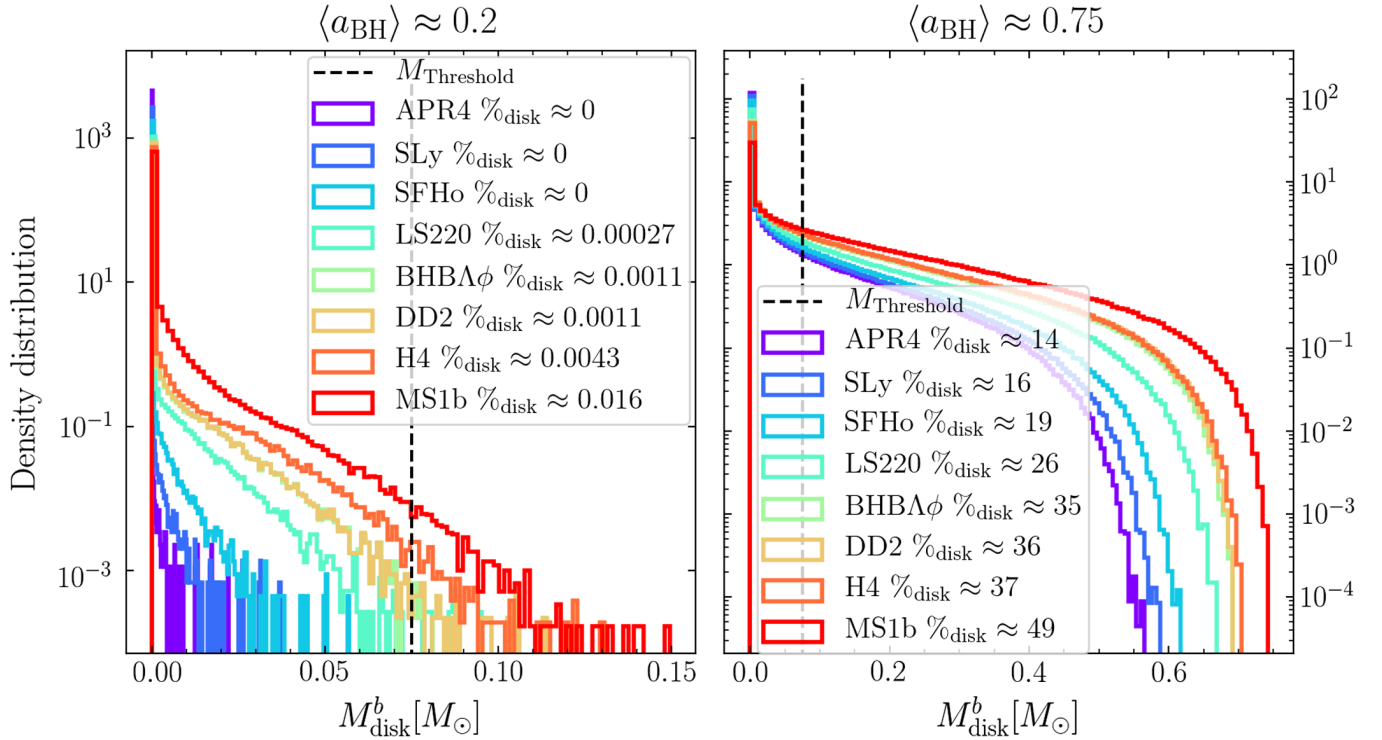
FIG. 3. Remnant disk baryonic mass distribution for different EOSs and for low (left) and high (right) aligned BH spin distributions. The mass threshold represents the minimum mass of the disk that allows the production of SGRBs with 1 s duration. The percentage of binaries with disk mass bigger than the threshold is provided in the legend for each equation of state.

root-mean square velocity $v_\sigma = 15 \text{ km s}^{-1}$ for both electron-capture and core-collapse supernovae. Larger kicks would enable the merger of more massive BHNSs (moderate kicks do not break the binary but increase its eccentricity, shortening the merger time of massive BHNSs, see Ref. [49] for details), but would not affect the minimum BHNS mass (see Fig. 5 of Ref. [56]). In run CC15α5, the minimum (maximum) mass of a BH (NS) is set to $5 \, M_\odot$ ($2 \, M_\odot$). This assumption enforces the existence of a mass gap between BHs and NSs, which is suggested by dynamical mass measurements of compact objects in x-ray binaries [57,58]. BH spins are added by randomly drawing spin magnitudes $|a_{\text{BH}}| \in [0, 1]$ from a truncated Maxwellian distribution with root-mean square σ. In this Letter, we consider spins isotropically oriented with respect to the binary orbital plane with $\langle a_{\text{BH}} \rangle = 0.2$ as fiducial distribution or aligned spin distributions with $\sigma = (0.1, 0.35, 0.5, 0.7)$, corresponding to average values $\langle a_{\text{BH}} \rangle = (0.2, 0.5, 0.75, 0.95)$. The aligned spin distributions give *upper limits* to the isotropic spin distributions.

The population synthesis predicts BH component masses below $10 \, M_\odot$ distributed narrowly about $M_{\text{BH}} \sim 5 \, M_\odot$ and $M_{\text{BH}} \sim 8 \, M_\odot$ [59]. The population depends very weakly on the progenitors' metallicities for $Z \leq 0.002$, but for $Z \geq 0.003$ the smallest BHs are suppressed and only BHs with $M_{\text{BH}} \sim 8 \, M_\odot$ are found. This is a consequence of the dependence of the delay time (i.e., the time elapsed between the formation of the progenitor stars and the

BHNS merger) on the progenitor's metallicity: metal-rich progenitors have longer delay times than metal-poor ones and thus do not merge within the Hubble time, especially if the BH mass is small [60]. Additionally, NS masses $M_{\text{NS}} \gtrsim 1.3 \, M_\odot$ are favored.

In order to compute the merger remnant from the population, we choose a representative set of EOSs and calculate Λ on the NS population for each EOS. The remnant properties are then determined with Eq. (1) with the prescription of Eq. (3). Remnant masses are shown in Fig. 2, while additional plots are reported in the SM [39]. For metallicities $Z \leq 0.002$, we find a bimodal distribution around $M_\bullet \sim 7 \, M_\odot$ and $M_\bullet \sim 9 \, M_\odot$ independently from the EOS. Large metallicities produce only the more massive remnants. The remnant spins inferred from Eq. (1) and the isotropic or aligned spin population with $\langle a_{\text{BH}} \rangle \approx 0.2$ are distributed around $a_\bullet^z \sim 0.4$ with standard deviation ~ 0.1. As shown in the SM [39], the distributions we find track the populations generated by the population synthesis code. Quantifying the precise dependency of the BH mass distribution on the assumptions about core-collapse supernovae, natal kicks, and common-envelope efficiency is work left for a future study.

Using the model of Ref. [26], we estimate the baryonic mass of the remnant disk. Figure 3 shows the aligned low spin distribution resulting in $\gtrsim 99\%$ of the remnants with baryonic mass of the disk smaller than $M_{\text{threshold}}^b = 0.075(M_{\text{NS}}^b/1.5)M_\odot$ independently from the EOS. Disk

masses above $M_{\text{threshold}}^b$ are necessary to produce SGRBs of 1 s duration [61,62]. Remnants with significant disk masses are found for aligned spin distributions with $\langle a_{\text{BH}} \rangle \gtrsim 0.5$. In these cases, the largest disks are found for the stiff EOS corresponding to $\Lambda \gtrsim 1700$. Soft EOSs, corresponding to $\Lambda \lesssim 400$, give massive disks only for $\lesssim 20\%$ of the binaries and with $\langle a_{\text{BH}} \rangle \gtrsim 0.75$.

Conclusion.—Our results indicate light and moderately spinning BH remnants surrounded by low-mass accretion disks (type-II) as the most likely outcome for BHNS if $\Lambda \lesssim 1000$ and the BH has aligned spin $a_{\text{BH}} \lesssim 0.75$. The observation of GW170817 rules out NS with $\Lambda \gtrsim 1800$ ($\gtrsim 2600$) for the low-spin (high-spin) prior cases [63]. Similarly, large aligned spins might be disfavored by current GW binary observations [8]. Type-II GW signals are very similar to BBHs. For aligned spins, GW searches will lose less than 1% of events employing BBH templates [64]. On the other hand, estimating Λ from the GW will be challenging, and BHNS mergers might not set constraints on the EOS unless ringdown signatures are resolved [35]. Type-II mergers are also not expected to be accompanied by bright electromagnetic counterparts. Disk masses above $M_{\text{threshold}}^b$ are rare in our populations, unless BHNSs are characterized by large and aligned BH initial spins, very stiff EOS, and/or compact objects with mass 2–5 $M_\odot$ (i.e., within the mass gap suggested by x-ray binaries).

The BH remnant model constructed in this work will be used in GW models for BHNSs [30,32–34,36,65,66], as well as for modeling the counterparts; see, e.g., Refs. [67–71]. It will thus be one of the key building blocks for upcoming multimessenger analysis of BHNSs.

[1] S. Rosswog, Astrophys. J. **634**, 1202 (2005).
[2] K. Kyutoku, H. Okawa, M. Shibata, and K. Taniguchi, Phys. Rev. D **84**, 064018 (2011).
[3] F. Foucart, M. B. Deaton, M. D. Duez, L. E. Kidder, I. MacDonald, C. D. Ott, H. P. Pfeiffer, M. A. Scheel, B. Szilagyi, and S. A. Teukolsky, Phys. Rev. D **87**, 084006 (2013).
[4] F. Foucart, M. B. Deaton, M. D. Duez, E. O'Connor, C. D. Ott, R. Haas, L. E. Kidder, H. P. Pfeiffer, M. A. Scheel, and B. Szilagyi, Phys. Rev. D **90**, 024026 (2014).
[5] F. Foucart, R. Haas, M. D. Duez, E. O'Connor, C. D. Ott, L. Roberts, L. E. Kidder, J. Lippuner, H. P. Pfeiffer, and M. A. Scheel, Phys. Rev. D **93**, 044019 (2016).
[6] V. Paschalidis, Classical Quantum Gravity **34**, 084002 (2017).
[7] M. Bhattacharya, P. Kumar, and G. Smoot, Mon. Not. R. Astron Soc. **486**, 5289 (2019).
[8] B. P. Abbott *et al.* (LIGO Scientific and Virgo Collaborations), arXiv:1811.12907.
[9] K. Kyutoku, M. Shibata, and K. Taniguchi, Phys. Rev. D **82**, 044049 (2010); **84**, 049902(E) (2011).
[10] K. Kyutoku, K. Ioka, and M. Shibata, Phys. Rev. D **88**, 041503(R) (2013).
[11] K. Kyutoku, K. Ioka, H. Okawa, M. Shibata, and K. Taniguchi, Phys. Rev. D **92**, 044028 (2015).
[12] F. Foucart, M. D. Duez, L. E. Kidder, and S. A. Teukolsky, Phys. Rev. D **83**, 024005 (2011).
[13] K. Kawaguchi, K. Kyutoku, H. Nakano, H. Okawa, M. Shibata, and K. Taniguchi, Phys. Rev. D **92**, 024014 (2015).
[14] Z. B. Etienne, Y. T. Liu, S. L. Shapiro, and T. W. Baumgarte, Phys. Rev. D **79**, 044024 (2009).
[15] Z. B. Etienne, J. A. Faber, Y. T. Liu, S. L. Shapiro, K. Taniguchi, and T. W. Baumgarte, Phys. Rev. D **77**, 084002 (2008).
[16] Z. B. Etienne, Y. T. Liu, V. Paschalidis, and S. L. Shapiro, Phys. Rev. D **85**, 064029 (2012).
[17] Z. B. Etienne, V. Paschalidis, and S. L. Shapiro, Phys. Rev. D **86**, 084026 (2012).
[18] V. Paschalidis, Z. B. Etienne, and S. L. Shapiro, Phys. Rev. D **88**, 021504(R) (2013).
[19] M. Bejger, D. Gondek-Rosińska, E. Gourgoulhon, P. Haensel, K. Taniguchi, and J. L. Zdunik, Astron. Astrophys. **431**, 297 (2005).
[20] T. Dietrich, M. Ujevic, W. Tichy, S. Bernuzzi, and B. Brügmann, Phys. Rev. D **95**, 024029 (2017).
[21] M. Shibata and K. Taniguchi, Living Rev. Relativity **14**, 6 (2011).
[22] J. M. Bardeen, W. H. Press, and S. A. Teukolsky, Astrophys. J. **178**, 347 (1972).
[23] T. Hinderer, B. D. Lackey, R. N. Lang, and J. S. Read, Phys. Rev. D **81**, 123016 (2010).
[24] T. Damour and A. Nagar, Phys. Rev. D **81**, 084016 (2010).
[25] F. Foucart, Phys. Rev. D **86**, 124007 (2012).
[26] F. Foucart, T. Hinderer, and S. Nissanke, Phys. Rev. D **98**, 081501(R) (2018).
[27] B. Paczynski, Astrophys. J. **308**, L43 (1986).
[28] D. Eichler, M. Livio, T. Piran, and D. N. Schramm, Nature (London) **340**, 126 (1989).
[29] L.-X. Li and B. Paczynski, Astrophys. J. **507**, L59 (1998).
[30] B. D. Lackey, K. Kyutoku, M. Shibata, P. R. Brady, and J. L. Friedman, Phys. Rev. D **85**, 044061 (2012).
[31] F. Pannarale, E. Berti, K. Kyutoku, and M. Shibata, Phys. Rev. D **88**, 084011 (2013).
[32] F. Pannarale, E. Berti, K. Kyutoku, B. D. Lackey, and M. Shibata, Phys. Rev. D **92**, 084050 (2015).
[33] T. Hinderer *et al.*, Phys. Rev. Lett. **116**, 181101 (2016).
[34] A. Nagar, S. Bernuzzi, W. Del Pozzo, G. Riemenschneider, S. Akcay, G. Carullo, P. Fleig, S. Babak, K. W. Tsang, M. Colleoni *et al.*, Phys. Rev. D **98**, 104052 (2018).
[35] F. Pannarale, Phys. Rev. D **88**, 104025 (2013).
[36] F. Pannarale, Phys. Rev. D **89**, 044045 (2014).
[37] A. Buonanno, L. E. Kidder, and L. Lehner, Phys. Rev. D **77**, 026004 (2008).

[38] D. Radice, A. Perego, K. Hotokezaka, S. A. Fromm, S. Bernuzzi, and L. F. Roberts, Astrophys. J. **869**, 130 (2018).

[39] See Supplemental Material at http://link.aps.org/supplemental/10.1103/PhysRevLett.123.041102 for more details on the fitting formula, the fit for the GW luminosity peak and more information on the population synthesis simulations mentioned in the main text, which includes Refs. [40–43].

[40] X. Jiménez-Forteza, D. Keitel, S. Husa, M. Hannam, S. Khan, and M. Pürrer, Phys. Rev. D **95**, 064024 (2017).

[41] D. Keitel *et al.*, Phys. Rev. D **96**, 024006 (2017).

[42] F. Zappa, S. Bernuzzi, D. Radice, A. Perego, and T. Dietrich, Phys. Rev. Lett. **120**, 111101 (2018).

[43] C. L. Fryer, K. Belczynski, G. Wiktorowicz, M. Dominik, V. Kalogera, and D. E. Holz, Astrophys. J. **749**, 91 (2012).

[44] L. Bildsten and C. Cutler, Astrophys. J. **400**, 175 (1992).

[45] C. S. Kochanek, Astrophys. J. **398**, 234 (1992).

[46] E. Barausse and L. Rezzolla, Astrophys. J. **704**, L40 (2009).

[47] F. Hofmann, E. Barausse, and L. Rezzolla, Astrophys. J. **825**, L19 (2016).

[48] N. Giacobbo, M. Mapelli, and M. Spera, Mon. Not. R. Astron. Soc. **474**, 2959 (2018).

[49] N. Giacobbo and M. Mapelli, Mon. Not. R. Astron. Soc. **480**, 2011 (2018).

[50] N. Giacobbo and M. Mapelli, Mon. Not. R. Astron. Soc. **482**, 2234 (2019).

[51] M. Vogelsberger, S. Genel, V. Springel, P. Torrey, D. Sijacki, D. Xu, G. Snyder, S. Bird, D. Nelson, and L. Hernquist, Nature (London) **509**, 177 (2014).

[52] M. Vogelsberger, S. Genel, V. Springel, P. Torrey, D. Sijacki, D. Xu, G. Snyder, D. Nelson, and L. Hernquist, Mon. Not. R. Astron. Soc. **444**, 1518 (2014).

[53] D. Nelson, A. Pillepich, S. Genel, M. Vogelsberger, V. Springel, P. Torrey, V. Rodriguez-Gomez, D. Sijacki, G. F. Snyder, B. Griffen, F. Marinacci, L. Blecha, L. Sales, D. Xu, and L. Hernquist, Astron. Comput. **13**, 12 (2015).

[54] M. Mapelli, N. Giacobbo, E. Ripamonti, and M. Spera, Mon. Not. R. Astron. Soc. **472**, 2422 (2017).

[55] M. Mapelli and N. Giacobbo, Mon. Not. R. Astron. Soc. **479**, 4391 (2018).

[56] M. Mapelli, N. Giacobbo, F. Santoliquido, and M. C. Artale, Mon. Not. R. Astron Soc. **487**, 2 (2019).

[57] F. Özel, D. Psaltis, R. Narayan, and J. E. McClintock, Astrophys. J. **725**, 1918 (2010).

[58] W. M. Farr, N. Sravan, A. Cantrell, L. Kreidberg, C. D. Bailyn, I. Mandel, and V. Kalogera, Astrophys. J. **741**, 103 (2011).

[59] M. Mapelli and N. Giacobbo, Mon. Not. R. Astron. Soc. **479**, 4391 (2018).

[60] N. Giacobbo *et al.* (to be published).

[61] N. Stone, A. Loeb, and E. Berger, Phys. Rev. D **87**, 084053 (2013).

[62] F. Pannarale and F. Ohme, Astrophys. J. **791**, L7 (2014).

[63] B. P. Abbott *et al.* (LIGO Scientific Collaboration and Virgo Collaboration), Phys. Rev. X **9**, 011001 (2019).

[64] I. Harry, S. Privitera, A. Bohé, and A. Buonanno, Phys. Rev. D **94**, 024012 (2016).

[65] B. D. Lackey, K. Kyutoku, M. Shibata, P. R. Brady, and J. L. Friedman, Phys. Rev. D **89**, 043009 (2014).

[66] F. Pannarale, E. Berti, K. Kyutoku, B. D. Lackey, and M. Shibata, Phys. Rev. D **92**, 081504(R) (2015).

[67] H. K. Lee, R. A. M. J. Wijers, and G. E. Brown, Phys. Rep. **325**, 83 (2000).

[68] A. M. Beloborodov, Astrophys. J. **539**, L25 (2000).

[69] K. Kawaguchi, K. Kyutoku, M. Shibata, and M. Tanaka, Astrophys. J. **825**, 52 (2016).

[70] A. Perego, D. Radice, and S. Bernuzzi, Astrophys. J. **850**, L37 (2017).

[71] C. Barbieri, O. S. Salafia, A. Perego, M. Colpi, and G. Ghirlanda, Astron. Astrophys. **625**, A152 (2019).